Effect of Edge Convection on the H-Mode

D. A. D'Ippolito and J. R. Myra
Lodestar Research Corporation, 2400 Central Ave., Boulder, Colorado 80301

June 5, 1999; revised August 23, 1999

Presented at the 2nd Europhysics Workshop on the Role of Electric Fields in Plasma Confinement and Exhaust, June 19 - 20, 1999, Maastricht, The Netherlands

---

DOE/ER/54392-05 LRC-99-72

LODESTAR RESEARCH CORPORATION
Boulder • Cambridge • Los Alamos • Telluride

Effect of Edge Convection on the H-Mode

D. A. D'Ippolito and J. R. Myra
Lodestar Research Corporation, Boulder, Colorado

I. Introduction

This paper describes a theoretical model of convection in the tokamak edge plasma and its application to understand the effect of convection on the H-mode temperature pedestal and transport barrier. We are concerned here with the role of steady-state convection driven by poloidal and toroidal symmetry-breaking of the equilibrium (e.g. by applied potential modulations or by non-uniform particle and heat sources and sinks), not with turbulence-driven convection. Steady-state convective flows have been measured in the edge and SOL of several tokamaks, caused by spatially localized disturbances such as rf antennas and gas puffing [1-5]. In particular, there is a growing body of experimental evidence for strong dc (i.e. time independent) convection in the edge and SOL plasma during ICRF heating [6-11].

In the usual idealized picture of the H-mode, a layer of poloidally-uniform sheared flow $v_y(x)$ develops in the edge plasma during the L-H transition which reduces turbulent diffusion by breaking up large scale turbulent eddies. However, it is the thesis of this paper that even after the H-mode transition there may be some remaining poloidal non-uniformity in the equilibrium, and dc convection (i.e. two dimensional, non-turbulent $\mathbf{E} \times \mathbf{B}$ flows) may play a role in some parameter regimes of interest. We mention here some examples which motivate the present work:

(i) JET data [9, 10, 12-14] shows that under certain conditions H-mode properties such as the threshold power, the ratio of particle to energy confinement times τ_p/τ_E, the temperature pedestal height, and the ELM amplitude and repetition rate are significantly different for ICRF H-modes than for NBI H-modes. Some of these differences may be attributed to the absence of energetic particles in the edge plasma during ICRF heating [15], but others are thought to be due to ICRF-driven convection [9-10].

(ii) There are interesting parallels on JET between the effects of ICRF heating alone and gas puffing during NBI heating on the H-mode temperature pedestals, ELM amplitudes and repetition rates in JET. In the original JET configuration, under certain conditions either ICRF or gas puffing led to the appearance of grassy ELMs in otherwise ELM-free H-modes [16]. In the present JET configuration, the usual H-mode is ELMy, but there is again a similarity. The edge pressure pedestal and ELM amplitude are lower, and the ELM repetition rate higher, for lower $k_\parallel$ phasing during ICRF heating [13, 14] and for higher flow rates during gas puffing [17]. If the dominant effect is simply the cooling of the edge plasma [17], rf-induced convection is a possible candidate to explain the ICRF-induced edge cooling.

(iii) Recent measurements on Alcator C-MOD [18] suggest that non-diffusive transport may be responsible for a significant fraction of the radial particle and energy transport over a wide range of discharges. The nature of the convective transport merits further study.

(iv) The physics of the attractive "low particle confinement" (LPC) H-modes on JET [19] and the "enhanced D_α" (EDA) H-modes on C-MOD [20, 21] is not yet understood. These modes are triggered by enhanced neutral or impurity influxes, have comparable energy confinement to normal H-modes, but show a reduction of τ_p/τ_E by a factor of 3. Analysis of the EDA H-modes suggests that the edge gradients are relaxed by a continuous process rather than an intermittent one such as ELMs. The role of radiation-driven convection in such plasmas is an interesting question.

The present work is the first step in a program to explore the hypothesis that edge convection (induced by either potential or temperature perturbations) can play a role in modifying and possibly optimizing the H-mode. The theoretical approach described in this paper is valid for either applied potential or temperature perturbations, but the specific analysis considered here is the one relevant to ICRF experiments, in which the spatial variation of the rectified (dc) sheath potential at the antenna drives $\mathbf{E} \times \mathbf{B}$ convection in the SOL and edge plasmas [9, 10]. The SOL physics is modeled here by an applied spatial modulation $\tilde{\Phi}(y)$ of the electrostatic potential at the separatrix; this modulation is specified as a boundary condition (BC) to drive the $\mathbf{E} \times \mathbf{B}$ flow in the edge region. A linear and nonlinear analysis of the edge plasma response is carried out within the framework of a 2-field (Φ, T_e) Braginskii model. The main result of this paper is that strong edge convection can nonlinearly modify both the electron temperature and radial electric field profiles in the edge in ways that would be expected to affect the H-mode pedestal and transport barrier.

The plan of this paper is the following. The model equations are derived in Sec. II. An analytic solution in the limit of strong convection is given in Sec. III and the validity conditions of the model are discussed. Application of the strong edge convection model to the low-$k_\parallel$ ICRF H-modes on JET [9, 10] is given in Sec. IV, and it is shown that the present work supports our earlier conjecture that ICRF-driven convection is a good candidate to explain this H-mode data. A summary and discussion of other implications of the model is given in Sec. V.

II. The Edge Convection Model

The calculation is based on the following reduced set of Braginskii equations for the electrostatic potential Φ and electron temperature T:

$$\frac{c^2}{B^2} n m_i \frac{d}{dt} \nabla_\perp^2 \Phi = \nabla_\parallel J_\parallel \ , \tag{1}$$

$$\eta \ J_\parallel = -\nabla_\parallel \Phi + \frac{\alpha}{e} \nabla_\parallel T_e \ , \tag{2}$$

$$\frac{3}{2} n \frac{dT_e}{dt} - \nabla_\parallel \kappa_{\parallel e} \nabla_\parallel T_e - \nabla_\perp \kappa_{\perp e} \nabla_\perp T_e = 0, \tag{3}$$

where $\alpha = 1.71$, $d/dt = \partial/\partial t + \mathbf{v}_E \cdot \nabla$, $\mathbf{v}_E = (c/B)\, \mathbf{b} \times \nabla_\perp \Phi$, $n = n_e = n_i$ is the particle density, m_i is the ion mass, $T = T_e >> T_i$, $\Omega_i = eB/m_i c$ is the ion cyclotron frequency, η is the electrical resistivity, and $\kappa_\parallel$ and $\kappa_\perp$ are the parallel and perpendicular electron heat conductivies. The Braginskii description is valid when the edge plasma is sufficiently collisional to ensure that the

mean free path λ_{ii} satisfies $\lambda_{ii} < L_{||} \sim qR$. In writing Eqs. (1) - (3), we neglect $v_{||i}$ and T_i effects, treat n as a constant, and retain only the $\mathbf{E} \times \mathbf{B}$ nonlinearity to simplify the model. The neglect of the density evolution equation is made only for convenience and is not expected to change the conclusions reached here. The terms proportional to $J_{||}$ neglected in Eq. (3) are small in the parameter $\delta = (\rho_s/L_\perp)^2 (\omega_E/k_{||}^2\chi)$ discussed below. Radiation sink terms may be important in Eq. (3) when thermal perturbations are driving the convection, but they are not important for the case of convection driven by an externally applied potential perturbation, which is the application considered here. The result of these approximations is a 2-field model which, despite its simplicity, has a rich and interesting nonlinear behavior.

We treat the unperturbed H-mode equilibrium as one-dimensional in the radial coordinate x and consider the effect of applied convection, induced by the coupled (zero-frequency) perturbations $\Phi_1(x,y,z)$ and $T_1(x,y,z)$, where z is the coordinate along $\mathbf{B}$, and y is in the $\mathbf{e}_z \times \mathbf{e}_x$ direction perpendicular to $\mathbf{B}$. Either of these perturbations can be regarded as the source and the other the response; here, the magnitude of the driving perturbation is assumed to be given at the separatrix (or last closed flux surface). The effect of the perturbation in linear theory is to drive $\mathbf{E} \times \mathbf{B}$ convection in the edge plasma; in nonlinear theory, the coupling of the perturbations gives rise to a poloidally-averaged modification of the background 1D equilibrium. Thus, we expand each quantity Q in powers of the perturbation amplitudes, $Q = Q_0 + \varepsilon\, Q_1 + \varepsilon^2\, Q_2 \ldots$, where $Q_0(x)$ is the equilibrium quantity in the absence of convection, $Q_1 = Q_1(x)\, \exp(ik_y\, y + ik_{||}\, z)$ is the perturbation, and $Q_2(x)$ is the second-order surface-averaged nonlinear modification of the equilibrium. The present calculation neglects third order and higher nonlinear terms; the validity condition for this approximation is discussed below. Note that for $k_{\|} \approx (1/qR)$ the perturbations implicitly have toroidal dependence, which in the rf case is due to the finite toroidal extent of the antenna [10].

The basic equations (1) - (3) are linearized and the following dimensionless variables are introduced: $\bar{\Phi} = e\Phi_0/T_s$, $\tilde{\Phi} = e\Phi_1/T_s$, $\bar{T} = T_0/T_s$, $\tilde{T} = T_1/T_s$, $\bar{v} = v_0/c_s$, $\tilde{v} = v_1/c_s$, where n_s, T_s and $c_s = (T_s/m_i)^{1/2}$ are constants, taken here to be the values on the separatrix. We also define the electron parallel diffusivity $\chi = (T_s/n_s \eta\, e^2)$, and the normalized perpendicular and parallel thermal conductivities, $\chi_\perp = (2\kappa_\perp/3n_s)$ and $\chi_{||} = (2\kappa_{\|}/3n_s)$. Treating these transport coefficients as constants, the linearized set of equations becomes

$$\bar{\mathbf{v}}_E \cdot \nabla\, \rho_s^2 \nabla_\perp^2\, \tilde{\Phi} + \tilde{\mathbf{v}}_E \cdot \nabla\, \rho_s^2 \nabla_\perp^2\, \bar{\Phi} = -\chi\ \nabla_{\|}^2 (\tilde{\Phi} - \alpha\, \tilde{T}) \ , \tag{4}$$

$$\bar{\mathbf{v}}_E \cdot \nabla\, \tilde{T} - \bar{\mathbf{v}}_{*T} \cdot \nabla\, \tilde{\Phi} = \chi_\perp \nabla_\perp^2 \tilde{T} + \chi_{||} \nabla_{||}^2 \tilde{T} \ , \tag{5}$$

where $\rho_s = c_s/\Omega_i$ and the normalized $\mathbf{E} \times \mathbf{B}$ and diamagnetic velocities are defined by $\bar{\mathbf{v}}_E = c_s \rho_s\, \mathbf{b} \times \nabla_\perp \bar{\Phi}$ and $\bar{\mathbf{v}}_{*T} = c_s \rho_s\, \mathbf{b} \times \nabla_\perp \bar{T}$. Using the fact that the equilibrium quantities vary only in x and employing the ansatz for the perturbed quantities, Eqs. (4) and (5) can be put in the form

$$i\, [\, \omega_E\, \rho_s^2 \nabla_\perp^2\, \tilde{\Phi} - \rho_s^2\, \omega_E''\, \tilde{\Phi}] = k_{||}^2\, \chi\ (\tilde{\Phi} - \alpha\, \tilde{T}) \, , \tag{6}$$

$$i\, [\omega_E\, \tilde{T} - \omega_{*T}\, \tilde{\Phi}\,] = \chi_\perp \nabla_\perp^2 \tilde{T} - k_{||}^2\, \chi_{||} \tilde{T} \ , \tag{7}$$

where a prime denotes d/dx, $\omega_E = k_y v_{Ey}$, and $\omega_{*T} = k_y v_{*Ty}$. Note that the perturbations $\tilde{\Phi}$ and $\tilde{T}$ are coupled by the thermoelectric force in the vorticity equation (6) and by the ω_{*T} drift in the temperature equation (7). We treat $k_\parallel$ as constant in the convective layer and assume that it is of order $k_\parallel \sim k_y (L_x/qR)$, where L_x is the radial width of the layer, q is the safety factor and R is the major radius.

The linearized Eqs. (6) and (7) are expanded in the parameter $\delta = (\rho_s/L_\perp)^2 (\omega_E/k_\parallel^2\chi)$, where $\delta << 1$ holds for typical edge plasma parameters. To lowest order in δ, the LHS of Eq. (6) vanishes and $J_\parallel = 0$, so that $\tilde{\Phi} = \alpha \tilde{T}$ in this order. Thus, there is a symmetry between potential and temperature perturbations in this model due to the thermoelectric force. The results of the δ expansion to first order are

$$\tilde{\Phi}^{(0)} = \alpha \tilde{T}^{(0)} \ , \tag{8a}$$

$$\tilde{\Phi}^{(1)} - \alpha \tilde{T}^{(1)} = i \frac{\rho_s^2}{k_\parallel^2 \chi} [\omega_E \nabla_\perp^2 \tilde{\Phi}^{(0)} - \omega_E'' \tilde{\Phi}^{(0)}] , \tag{8b}$$

$$\chi_\perp \nabla_\perp^2 \tilde{T}^{(0)} - k_\parallel^2 \chi_\parallel \tilde{T}^{(0)} = i [\omega_E \tilde{T}^{(0)} - \omega_{*T} \tilde{\Phi}^{(0)}] , \tag{9a}$$

$$\begin{aligned} \chi_\perp \nabla_\perp^2 \tilde{T}^{(1)} - k_\parallel^2 \chi_\parallel \tilde{T}^{(1)} &= i [\omega_E \tilde{T}_1^{(1)} - \omega_{*T} \tilde{\Phi}_1^{(1)}] , \\ &= i (\omega_E - \alpha \omega_{*T}) \tilde{T}^{(1)} + \frac{\rho_s^2 \omega_{*T}}{k_\parallel^2 \chi} [\omega_E \nabla_\perp^2 \tilde{\Phi}^{(0)} - \omega_E'' \tilde{\Phi}^{(0)}] . \end{aligned} \tag{9b}$$

Here the superscripts in parentheses indicate the order in δ; the expansion of the vorticity equation (6) yields Eq. (8) and that of the temperature equation (7) gives Eq. (9). Carrying out the expansion to first order in δ is sufficient for the nonlinear theory to order $\varepsilon^2 = |\tilde{\Phi}|^2$.

In the nonlinear analysis, the $\mathbf{E} \times \mathbf{B}$ nonlinearities on the LHS of Eqs. (1) and (3) couple the perturbations to produce a net surface-averaged modification of the underlying equilibrium. Denoting the nonlinear terms in the vorticity and temperature equations by S_V and S_T, respectively, we evaluate them to order $|\tilde{\Phi}|^2$ as follows

$$\begin{aligned} S_v &\equiv -\frac{1}{4} \nabla \cdot [c_s \rho_s \mathbf{b} \times \nabla_\perp \tilde{\Phi}^* \ \rho_s^2 \nabla_\perp^2 \tilde{\Phi}] + cc \ , \\ &= -\frac{1}{4} k_y c_s \rho_s^3 \nabla_x (i \tilde{\Phi}^* \nabla_\perp^2 \tilde{\Phi} + cc) \ . \end{aligned} \tag{10}$$

$$\begin{aligned} S_T &\equiv -\frac{1}{4} \nabla \cdot [c_s \rho_s \mathbf{b} \times \nabla_\perp \tilde{\Phi}^* \tilde{T}] + cc \ , \\ &= -\frac{1}{4} k_y c_s \rho_s \nabla_x (i \tilde{\Phi}^* \tilde{T} + cc) \ . \end{aligned} \tag{11}$$

Here, cc denotes the complex conjugate, which is used to obtain the flux-surface average. In terms of the δ ordering, the lowest order solutions $\{\tilde{\Phi}^{(0)}, \tilde{T}^{(0)}\}$ obtained from Eqs. (8a) and (9a) combine to give a non-vanishing contribution to S_v but do not give a finite contribution to S_T.

The first non-vanishing contribution to S_T comes in order δ from the terms ($i\,\tilde{\Phi}^{(0)*}\ \tilde{T}^{(1)} + i\ \tilde{\Phi}^{(1)*}\ \tilde{T}^{(0)} + cc$) using Eqs. (8b) and (9b). The validity condition for neglecting nonlinear terms higher than second order is discussed in Sec. III.

Substituting the linear solutions for $\tilde{\Phi}$ and $\tilde{T}$ to order δ into the nonlinear terms in Eqs. (10) and (11) and carrying out the spatial averaging, we obtain the following set of modified equilibrium equations for the vorticity and the electron temperature:

$$\frac{\partial}{\partial t}\rho_s^2\nabla_\perp^2\bar{\Phi} + \mu_\theta\rho_s^2\nabla_\perp^2(\bar{\Phi}-\bar{\Phi}_b) = \frac{k_y c_s \rho_s^3}{2\chi_\perp}\nabla_x\left[\,|\tilde{\Phi}|^2\,(\omega_E - \alpha\,\omega_{*T})\,\right], \qquad (12)$$

$$\frac{\partial}{\partial t}\bar{T} - \chi_\perp\nabla_\perp^2(\bar{T}-\bar{T}_b) = -\frac{k_y c_s \rho_s^3}{2\alpha k_\parallel^2 \chi\,\chi_\perp}\nabla_x\left[\,|\tilde{\Phi}|^2\,(k_\parallel^2\,\chi_\parallel\,\omega_E - \chi_\perp\omega_E'')\,\right]. \qquad (13)$$

In the vorticity equation, Eq. (12), a neoclassical damping term was included to provide a steady state solution in the limit of small convection ($\tilde{\Phi}\to 0$). The neoclassical damping coefficient is given by $\mu_\theta \approx (v_i/qR)^2\,\nu_{ii}^{-1}$ in the Braginskii regime, where v_i is the ion thermal velocity and ν_{ii} is the ion-ion collision frequency. The functions $\bar{\Phi}_b(x)$ and $\bar{T}_b(x)$ are inputs to the present theory and denote the steady state solution in the absence of the nonlinear terms; these functions can be regarded as source terms representing the other physical effects not explicitly considered in our model, such as turbulent generation of $\mathbf{E}\times\mathbf{B}$ flow shear. For present purposes these extra terms are included merely to indicate the mathematical structure of the problem; we restrict the discussion in this paper to the physics of the nonlinear terms on the right hand side (RHS) of these equations.

The equilibrium equations must be supplemented by an equation to determine the radial penetration of $\tilde{\Phi}(x)$ into the edge plasma for given boundary conditions (BCs). This equation is obtained by substituting the lowest order linearized result $\tilde{\Phi} = \alpha\,\tilde{T}$ [see Eq. (8a)] into Eq. (7). The linear eigenmode equation can be put into the form

$$(1 - L_0^2\nabla_\perp^2)\,\tilde{\Phi} = -i\,[L_0^2(\omega_E - \alpha\,\omega_{*T})/\chi_\perp]\,\tilde{\Phi}, \qquad (14)$$

where we have defined $L_0 = (\chi_\perp/k_\parallel^2\chi)^{1/2}$ and use the fact that $\chi_\parallel \approx \chi$. For typical edge parameters the individual drift terms on the RHS of Eq. (14) are large compared to the terms on the LHS, but the sum of the two drifts can be neglected, because in Sec. III we will show that the strongly nonlinear regime imposes the constraint that $\omega_E = \alpha\ \omega_{*T}$. Thus, we find that a potential modulation $\tilde{\Phi}$ imposed at the separatrix will exponentially decay into the edge plasma with the radial scale length L_0. Combining the definitions of L_0 and $k_\parallel = k_y\,(L_0/qR)$, one finds the scaling that $L_0 = (qR/k_y)^{1/2}\,(\chi_\perp/\chi)^{1/4}$.

Equations (12) - (14) constitute our edge convection model.

III. Nonlinear Equilibrium Analysis

A complete analysis of the convective equilibrium problem would entail numerical solution of the steady-state solutions of Eqs. (12) - (14) with appropriate BCs. These equations can be rewritten in a simpler form, in terms of the drift frequencies and a normalized perturbation amplitude $\tilde{\Phi}_n \equiv \tilde{\Phi} / \tilde{\Phi}_c$ as follows:

$$\mu\, L_0\, \nabla_x\, (\omega_E - \omega_{Eb}) \;=\; L_0\, \nabla_x\, [\, |\tilde{\Phi}_n|^2\, (\omega_E - \alpha\, \omega_{*T})\,]\;, \tag{15}$$

$$\alpha\, L_0\, \nabla_x\, (\omega_{*T} - \omega_{*Tb}) \;=\; L_0\, \nabla_x\, [\, |\tilde{\Phi}_n|^2\, (\omega_E - L_0^2\, \omega_E'')\,]\;, \tag{16}$$

$$i\, [L_0^2\, (\omega_E - \alpha\, \omega_{*T}) / \chi_\perp]\, \tilde{\Phi}_n \;+\; (\, 1 - \, L_0^2\, \nabla_\perp^2\,)\, \tilde{\Phi}_n \;= 0, \tag{17}$$

where $\tilde{\Phi}_c^2 = 2\chi_\perp^2 / k_y^2 c_s^2 \rho_s^4$ and $\mu = (\mu_\theta \rho_s^2 / \chi_\perp)$. In Eqs. (15) and (16), the drift frequencies ω_{Eb} and ω_{*Tb} are defined based on the background profiles $\bar{\Phi}_b$ and $\bar{T}_b$. Integrating Eqs. (15)-(16) once and neglecting the small drift terms in Eq. (17), we obtain

$$\mu\, (\omega_E - \omega_{Eb}) \;=\; |\tilde{\Phi}_n|^2\, (\omega_E - \alpha\, \omega_{*T})\;, \tag{18}$$

$$\alpha\, (\omega_{*T} - \omega_{*Tb}) \;=\; |\tilde{\Phi}_n|^2\, (\omega_E - L_0^2\, \omega_E'')\;, \tag{19}$$

$$(\, 1 - L_0^2\, \nabla_\perp^2\,)\, \tilde{\Phi}_n \;= 0, \tag{20}$$

It is evident that the nonlinear effect of the convection, represented by the terms on the RHS of Eqs. (18) and (19), is to drive ω_E and ω_{*T} away from their former equilibrium values ω_{Eb} and ω_{*Tb}.

The convective equilibrium modifications occur in a layer whose width is given by the solution of Eq. (20). With the BCs that the separatrix value of $\tilde{\Phi}_n$ is specified (determined by the SOL physics) and that $\tilde{\Phi}_n \to 0$ in the core ($x \to -\infty$), Eq. (20) yields an exponential solution:

$$\tilde{\Phi}_n(x) = \tilde{\Phi}_n(x_s)\; \exp[(x - x_s)/L_0]. \tag{21a}$$

We will see below that for some parameters the nonlinear model can be applied in the large-$\tilde{\Phi}$ regime ($\tilde{\Phi}_n >> 1$). Defining the convective layer as the radial region for which $\tilde{\Phi}_n(x) > 1$ and using Eq. (21a), we obtain the following estimate for the layer width Δx_c

$$\Delta x_c = L_0 \ln \tilde{\Phi}_n(x_s) = \; L_0 \ln (\tilde{\Phi}_s / \tilde{\Phi}_c), \tag{21b}$$

where we recall that $\tilde{\Phi} \equiv e\Phi_1/T_s$ and define $\tilde{\Phi}_s \equiv \tilde{\Phi}(x_s)$.

A numerical solution of Eqs. (18) and (19) has not been carried out, but we can obtain an interesting analytic solution in the limit of strong convection ($\tilde{\Phi}_n \to \infty$). In this limit (which is appropriate to some rf experiments) the nonlinear terms on the RHS of Eqs. (18) and (19) dominate the solution, and the modified equilibrium is given by

$$\omega_E = \alpha\, \omega_{*T}\;, \tag{22a}$$

$$L_0^2\, \omega_E'' - \omega_E \;= 0\;. \tag{22b}$$

The important general point to note from this solution is that *in the strong convection limit the vorticity and temperature equations impose additional constraints relating the equilibrium flux-surface-averaged E_x and T profiles.* Equation (22b) implies that the equilibrium profile $E_x(x)$ varies on the same scale L_0 as the convection, and Eq. (22a) then relates the magnitude and sign of E_x to $\nabla_x T$. These constraints are not present in the usual H-mode edge plasma.

Before proceeding with the analysis, it is necessary to discuss the conditions under which the strong convection limit is valid, given the fact that terms of order $|\tilde{\Phi}|^3$ and higher were neglected in Eqs. (10) and (11). We have investigated this question to first order in the small parameter δ. It can be shown from the general nonlinear equations that the condition for neglect of nonlinear terms higher than quadratic is $\tilde{\mathbf{v}}_E \cdot \nabla\ (\tilde{\Phi} - \alpha\, \tilde{T}) \ll \chi_\perp \nabla_\perp^2 \tilde{T}$, which implies $\tilde{\Phi} \ll \tilde{\Phi}_c^2$, whereas the strong convection limit used to obtain Eqs. (22) is valid when $\tilde{\Phi} \gg \tilde{\Phi}_c$. Thus, the large-$\tilde{\Phi}$ limit of the present theory is valid when

$$1 \ll \tilde{\Phi}_c \ll \tilde{\Phi} \ll \tilde{\Phi}_c^2 \ , \qquad (23)$$

where $\tilde{\Phi}_c^2 = 2\chi_\perp^2 / k_y^2 c_s^2 \rho_s^4$. Thus, the large–$\tilde{\Phi}$ limit represents a physically realizable regime, which is relevant for some experimental parameters of interest. For example, letting $k_y = 2\pi/L_y$ and taking the parameters $L_y = 10$ cm, $\chi_\perp = 5 \times 10^3\ \mathrm{cm^2\,s^{-1}}$, $n_s = 2 \times 10^{13}\ \mathrm{cm^{-3}}$, and $T_s = 50$ eV, we find that $\tilde{\Phi}_c = 3.1$ and $\tilde{\Phi}_c^2 = 9.8$, so that the large–$\tilde{\Phi}$ model can be applied in a reasonable range consistent with Eq. (23). Using the expression for L_0 given after Eq. (14) and the definition of Δx_c in Eq. (21b), these parameters also yield the estimates $L_0 = 0.7$ cm and $\Delta x_c = 1.2$ cm for $\tilde{\Phi}_s/\tilde{\Phi}_c = 5$. Thus, the convective layer spans a significant fraction of the distance between the separatrix and the transport barrier in a typical H-mode plasma. Such large edge potentials can easily be obtained by either antenna rf sheath effects [10] or electrode biasing [22].

Having shown that the large-convection model is at least marginally valid for typical parameters, we turn to the solution of the model equations. The third-order system of equations, Eqs. (22), has been solved for $E_x(x)$ and $T(x) = T_e(x)$ on the interval $x_m < x < x_s$ subject to the following BCs:

$$T(x_m) = T_m, \quad T(x_s) = T_s, \quad E_x(x_s) = E_s, \qquad (24)$$

where x_s denotes the radial position of the separatrix and $x_m < x_s$ denotes a point in the edge plasma where the convection has decayed to a negligible level; the SOL is located at $x > x_s$. The motivation for these BCs is the following: (i) the temperature T_m is set by core and edge physics outside the convective layer; (ii) the separatrix temperature T_s is assumed to be set by a combination of atomic physics and by convective cooling in the SOL; and (iii) E_s is determined by the sheath physics in the SOL. Previous simulations [10] of the SOL sheath physics show E_s can have either sign, depending on the antenna voltage and the antenna-plasma separation. Other means of biasing, such as electrodes [22], can also produce either sign of E_s. Given the BCs in Eq. (24), the analytic solution of Eqs. (22) may be written as

$$E_x(x) = E_s \cosh\left(\frac{x_s - x}{L_0}\right) + \frac{\alpha C_T}{L_0} \sinh\left(\frac{x_s - x}{L_0}\right) , \qquad (25a)$$

$$T(x) = T_s + C_T \left[\cosh\left(\frac{x_s - x}{L_0}\right) - 1\right] + \frac{L_0 E_s}{\alpha} \sinh\left(\frac{x_s - x}{L_0}\right) , \qquad (25b)$$

$$C_T = \frac{\Delta T - \frac{L_0 E_s}{\alpha} \sinh\left(\frac{x_s - x_m}{L_0}\right)}{\cosh\left(\frac{x_s - x_m}{L_0}\right) - 1} , \qquad (25c)$$

where $\Delta T = T_m - T_s$ is the change in the electron temperature across the convective layer.

This solution shows that a variety of behaviors are possible in different regions of parameter space. As E_s and ΔT are varied at fixed T_s, one obtains regimes of nonlinear cooling or heating of the convective layer, regimes of non-monotonic T(x), and unphysical regimes ($T < 0$). The most experimentally-relevant regime is obtained for moderate E_s and is illustrated by the equilibrium profiles $E_x(x)$ and $T_e(x)$ shown in Figs. (1a) and (1b). Here we have used the parameters given after Eq. (23) with $E_s = 0$, $T_s = 50$ eV and $T_m = 200$ eV. Note that the convection forces $E_x > 0$ in the layer, the opposite sign from that found in the normal H-mode transport barrier and in the direction to increase ion losses. A reversal in the sign of E_x during ICRF heating has been observed on TEXTOR [23], as discussed in Sec. V. In Fig. (1b), the solution for T(x) in Eq. (25b) (solid line) is compared with the solution of $\nabla_x^2 T = 0$ (dashed line), which is valid in the absence of convection and other heat sources and sinks. For the parameters used here, it is seen that the effect of strong convection on the temperature is to nonlinearly cool the edge by flattening the T profile near the separatrix, and thus to make the edge plasma more resistive.

For general parameters, the constraint on the electric field can be further elucidated by taking the broad layer limit $\Delta x_c/L_0 = \ln(\tilde{\Phi}_s/\tilde{\Phi}_c) \to \infty$. In this limit, Eqs. (25) yield the analytic result that

$$E_m \approx \alpha \Delta T/L_0 - E_s . \qquad (26)$$

Thus, the modification of E_x saturates as the convective layer broadens. Typically the first term on the RHS of Eq. (26) is the largest and E_m is positive. The dependence on E_s in Eq. (26) may be important in understanding earlier JET rf experiments, as discussed in Sec. IV. It can also be shown that the shear $E_x'(x)$ is confined to boundary layers of width L_0, viz. $E_m' \approx -E_m/L_0$ in the layer near x_m and $E_s' \approx E_s/L_0$ near x_s. Away from the boundary layers, an asymptotic expansion in $\Delta x/L_0$ yields the result that

$$L_0 E_x'(x) = -\exp\left[-\left(\frac{x - x_m}{2L_0}\right)\right]\left(\frac{\alpha \Delta T}{L_0} - E_s\right) , \qquad (27)$$

where the exponential factor in Eq. (27) is small in the asymptoptic theory. Thus, except in narrow boundary layers, the shear E_x' is typically small in most of the convective layer. For typical experimental parameters, $\Delta x_c/L_0$ is of order unity and the asymptotic solution is not formally valid. Nevertheless, the shear E_x' is strongly modified [see Fig. (1a)] compared to the

normal H-mode case where E_x typically changes sign in the edge. Thus, strong convection can modify the effective electric field and $\mathbf{E} \times \mathbf{B}$ shear "seen" by the edge turbulence.

To summarize this section, our model suggests that strong convection can modify the H-mode pedestal and transport barrier region by changing the electric field and electron temperature profiles near the separatrix. These modifications occur in a layer of width Δx_c given by Eq. (21b). The convection may be expected to modify the H-mode transport barrier significantly if Δx_c is comparable to the distance Δx_b between the barrier and the separatrix; however, even when $\Delta x_c << \Delta x_b$, the convection changes the boundary condition near the separatrix and may still have an effect on the H-mode equilibrium.

IV. Application to RF Biasing on JET

As a first application of this theory, we will show that it provides a specific physical mechanism to support our earlier suggestion [10] that rf-driven convection was responsible for the differences between ICRF H-modes with low- and high-$k_{||}$ phasing on JET [9, 10]. In a series of experiments carried out on JET in 1991 with the A1 (two-strap) antennas, it was shown for the first time that H-modes could be obtained by ICRF alone in either 0- or π-phasing of the current straps. The H-modes obtained with π-phasing (high $k_{||}$) were identical to those obtained with neutral beams, but those obtained with 0-phasing (low $k_{||}$) had an increased power threshold, degraded H-mode confinement, longer duration, and did not suffer radiative collapse. In the π-phasing case, the line-averaged density was found to increase with time until a catastrophic spike in the radiated power terminated the discharge (due to a marfelike radiation instability in the X-point region), but this did not occur in the 0-phasing case. A unique and crucial aspect of this experiment was the use of high power ICRF heating in 0-phasing together with a feedback system that reduced the antenna-plasma separation to maintain constant antenna loading across the L$\rightarrow$H transition, resulting in small antenna-plasma separations (~ 1 cm) during the H-mode phase. The interesting question posed by these experiments was to find a physical mechanism whereby the phasing of the antenna could affect global H-mode properties such as the threshold power and confinement time.

We proposed the following explanation [10] for these observations, which the present work supports and extends. The formation of rf sheaths on the antenna [23] leads to a large time-averaged ("rectified") potential in the SOL which has the appropriate spatial dependence to drive $\mathbf{E} \times \mathbf{B}$ convection. The magnitude of the dc sheath potential and the associated convection have a strong phasing dependence (small in π phasing, large in 0-phasing). A 2D simulation of the convective flow in Ref. 10 showed that the antenna-driven convective cells could penetrate to the separatrix and modulate the electrostatic potential at the plasma boundary, if the antenna voltage were large enough and the antenna-plasma separation were small enough. For typical JET parameters, the simulation found that an antenna-plasma separation of less than 1.5 cm was sufficient to strongly perturb the separatrix potential for the large (~ kV) antenna sheath potentials obtained at high power in 0 phasing. This theoretical estimate was comparable to the

measured antenna-plasma separation for H-modes with 0-phasing. Moreover, an analysis of the data showed a convective flattening of the density profile in 0-phasing which was absent in π-phasing. Thus, it was conjectured that the strong convection driven by the rf sheath potential reduced the edge particle and energy confinement inside the separatrix leading to the observed global H-mode properties.

The nature of the modification of the H-mode equilibrium inside the separatrix was not addressed in our earlier work. The present model suggests that an important aspect is the constraint imposed on the equilibrium E_x. It is now well estabished by both measurements and simulations [e.g. see Ref. 24] that a crucial part of the L→H transition is the modification of the radial profile, $E_x(x)$, by the turbulence-induced sheared flow; it is found that after the transition E_x becomes strongly negative inside the separatrix and the flow shear proportional to $dE_x(x)/dx$ increases, thereby enhancing the ion confinement and reducing turbulent diffusion. The present model implies that strong edge convection tends to oppose both of these processes. To illustrate this effect more quantitatively, we estimate the values of E_s and E_m that would have been obtained in the JET experiments described above. The first step is to model the field-line-averaged dc SOL potential as the sum of Bohm and rf sheath contributions:

$$\bar{\Phi}(x) = \frac{3T_s}{e} \exp\left[\frac{(x_s - x)}{L_T}\right] + \Phi_a \exp\left[\frac{(x - x_s - \Delta x_a)}{\delta_e}\right], \qquad (28)$$

where L_T is the temperature gradient scale length in the SOL, Φ_a is the rectified sheath potential at the antenna, $\Delta x_a = x_a - x_s$ is the antenna-plasma separation, and $\delta_e = c/\omega_{pe}$ is the electron skin depth. In Eq. (28), the Bohm sheath potential decays like $T_e(x)$ in the SOL, and the rf sheath potential contribution grows as the antenna is approached ($x \to x_a$). We estimate E_s as $E_s = -\nabla_x \bar{\Phi}$)(x_s), and E_m is obtained by substituting this value of E_s into the strong convection result, Eq. (26). Note from Eq. (28) that E_s is positive for $\Delta x_a \to \infty$ and E_s is negative for $\Delta x_a \to 0$. Thus, E_s and E_m may be regarded as functions of the antenna-plasma separation Δx_a with all other parameters fixed for simplicity. In Fig. 2, E_s and E_m are plotted vs Δx_a for the parameters Φ_a = 1000 V (typical of 0-phasing), L_T = 1 cm, δ_e = 0.4 cm, ΔT = 150 eV, and L_0 = 0.7 cm. The plot shows that E_s is negative for Δx_a < 1.1 cm because of the effect of the rf sheath potential. Figure 2 also shows that E_m > 200 V/cm for Δx_a = 3 cm and becomes substantially larger for Δx_a < 1.5 cm. Thus, for typical SOL and edge parameters, the value of E_m in Fig. 2 is comparable to (and has the *opposite sign* from) the values of $|E_r|$ inside the separatrix obtained in recent measurements on DIII-D and in self-consistent simulations of edge turbulence [24]. By constraining the radial electric field to have the opposite sign from the normal H-mode, the convection in the edge plasma provides a simple mechanism for degrading the plasma confinement, as observed in the early JET ICRF H-mode experiments. The dependence on phasing (through Φ_a) and plasma position (through Δx_a) agree qualitatively with the experimental observations.

V. Summary and Discussion

For collisional edge plasmas described by the Braginkii equations, we have derived a set of nonlinear model equations (see Sec. II) describing the interaction of steady-state $\mathbf{E} \times \mathbf{B}$ convection with the tokamak edge plasma electric field and electron temperature. The convection can be driven by a spatial modulation of either the equilibrium edge potential Φ (e.g. due to ICRF-driven sheath effects) or the edge T (e.g. due to gas puffing). Application to the former case was illustrated here. These zero-frequency perturbations satisfy $\tilde{\Phi} = \alpha\ \tilde{T}$ to lowest order, because of the thermoelectric force. The quadratic interactions between $\tilde{\Phi}$ and $\tilde{T}$ give nonlinear terms in the flux-surface-averaged vorticity and electron temperature equations which can modify the equilibrium profiles in the convective layer. An analytic solution of the nonlinear equations in the limit of strong convection (see Sec. III) imposes additional constraints on the profiles T(x) and $E_x(x)$. Solution of these equations in the convective region for reasonable choices of the BCs implies that the convection can produce significant cooling, a reversal in the sign of E_x, and a modification in the $\mathbf{E} \times \mathbf{B}$ shear in the edge plasma inside the separatrix.

Combined with the SOL model of rf-driven convection in Ref. [10], this work provides a mechanism to explain the experimental dependence of the ICRF H-mode on the JET A1 antenna phasing [9, 10], as discussed in Sec. IV. For the JET antenna geometry, estimates show that the strong convection limit corresponds to low $k_{||}$ phasing of the ICRF antennas and that the modifications of E_x and its shear (leading to reduced plasma confinement) are larger for small antenna-plasma separation. In both respects, the theoretical model is consistent with the data.

The present work may also be relevant to other experimental observations described in Sec. I. First, the theory suggests two possible causes for the parallels between ICRF and gas puffing. In linear theory, the lowest-order result that $\tilde{\Phi} = \alpha\ \tilde{T}$ implies that either antenna-biasing effects or radiation localized near the X-point could drive convection in the edge plasma. The nonlinear theory shows that, in some parameter regimes, ICRF-driven convection can cool the edge plasma, just as occurs with gas puffing. It should be noted that the nonlinear convective cooling mechanism has the correct phasing dependence to explain the recent JET ICRF ELM data [13, 14]. The rf sheath potential, and hence the convection, increases as $k_{\|}$ is reduced; thus, one would expect cooler and more resistive edge plasmas for low $k_{||}$ if the convection is significant. This dependence agrees qualitatively with the data: the edge pressure and ELM amplitude drop and the repetition rate increases for smaller $k_{||}$.

The theoretical prediction that strong edge convection constrains the edge electric field profile, reversing the sign of E_x and modifying the $\mathbf{E} \times \mathbf{B}$ shear and resulting turbulence level, may be relevant to TEXTOR measurements of the edge electric fields. For typical parameters, our theory predicts that the sign of E_x is positive in the convective layer, which should in turn reduce the ion confinement in the edge plasma. The connection between $E_x > 0$ and reduced particle confinement has been observed in two experiments on TEXTOR [22, 23]. In the first experiment [23], probe measurements showed that ICRF heating reversed the sign of E_x in the edge plasma. The measured E_x was negative inside the last-closed-flux-surface (LCFS) during standard Ohmic operation, but E_x became positive during ICRF heating. The corresponding DC

radial particle flux inside the LCFS increased by more than an order of magnitude during ICRF heating (dominating the turbulent flux) and the spatial dependence of the radial and poloidal fluxes suggested the existence of macroscopic stationary convective cells in the edge plasma. In the second series of experiments, the H-mode biasing experiments on TEXTOR [22], also showed a clear asymmetry between H-modes produced with positive and negative E_x. The two cases showed comparable energy confinement, but the ratio of τ_p/τ_E was about three times lower for $E_x > 0$. A similar reduction in τ_p/τ_E was obtained in the "low particle confinement" H-modes on JET [19] and the "Enhanced D_α" H-modes on C-MOD [20, 21]. It is interesting to speculate that edge convection might play a role in these regimes. To apply our theory to these experiments, we will need to include an equation for the density evolution in order to distinguish between the effects of convection on energy and particle transport; also, energy sources and sinks (such as radiation) should be added to the temperature equation to drive thermal convection.

In summary, this work has shown that symmetry-breaking perturbations of the edge plasma potential and temperature can have important consequences for the H-mode edge profile evolution and, by implication, for its confinement and stability properties.

Acknowledgements

The authors would like to thank Ved Bhatnagar and Jean Jacquinot for providing us with unpublished JET data and for stimulating conversations which have motivated the work reported here. We would also like to thank Guido Van Oost for suggesting the relevance of this work to the TEXTOR experiments. This work was supported by the U.S. Department of Energy under Contract No. DE-FG03-97ER54392.

References

1. B. LaBombard and B. Lipschultz, Nucl. Fusion **27**, 81 (1987).
2. A. V. Nedospasov, S. S. Bychkov, V. V. Gaponov et al., J. Nucl. Mater. **176 & 177**, 169 (1990).
3. V. P. Budaev, L. M. Bobomolov, B. V. Borovsky, et al., J. Nucl. Mater. **176 & 177**, 705 (1990).
4. G. R. Tynan, L. Schmitz, R. W. Conn, et al., Phys. Rev. Lett. **68**, 3032 (1992).
5. H. Ohtsuka, JFT-2M Group, Nucl. Fusion **33**, 523 (1993).
6. R. A. Moyer, R. Van Nieuwenhove, G. Van Oost, D. Bora, et al., J. Nucl. Mater. **176 & 177**, 293 (1990).
7. D. Bora, R. S. Ivanov, G. Van Oost, U. Samm, Nucl. Fusion **31**, 2383 (1991).
8. D. A. Diebold, R. Majeski, T. Tanaka, et al., Nucl. Fusion **32**, 2040 (1992).
9. J. Jacquinot and the JET Team, Plasma Phys. Controlled Fusion **33**, 1657 (1991).
10. D. A. D'Ippolito, J. R. Myra, J. Jacquinot, and M. Bures, Phys. Fluids B **5**, 3603 (1993).
11. D. A. D'Ippolito, J. R. Myra, J. H. Rogers, et al., Nucl. Fusion **38**, 1543 (1998).
12. V. P. Bhatnagar, et al., *Proceedings of the 24th EPS Conference on Controlled Fusion and Plasma Physics*, Berchtesgaden, Germany, Vol. **I**, p. 77 (1997).

13. V. P. Bhatnagar, private communication (1998).
14. D. A. D'Ippolito, J. R. Myra, V. P. Bhatnagar, and J. Jacquinot, in *Proceedings of the International Sherwood Fusion Theory Conference*, Atlanta, Georgia, March 23-25, 1998; ibid., Bull. APS **43**, 1755 (1998).
15. J. Lingertat, V. Bhatnagar, G. D. Conway, L-G Eriksson, et al., J. Nucl Mater. **266-269**, 124 (1999).
16. J. Jacquinot et al., Phys. Fluids B **4**, 2114 (1992).
17. G. M. Fishpool, Nucl. Fusion **38**, 1373 (1998).
18. M. V. Umansky, S. I. Krasheninnikov, B. LaBombard, and J. L. Terry, Phys. Plasmas **5**, 3373 (1998).
19. M. Bures, D. J. Campbell, N. A. C. Gottardi, J. J. Jacquinot, M. Mattioli, P. D. Morgan, D. Pasini, and D. F. H. Start, Nucl. Fusion **32**, 539 (1992).
20. Y. Takase, R. L. Boivin, F. Bombarda, et al., Phys. Plasmas **4**, 1647 (1997).
21. M. Greenwald, R. Boivin, P. Bonoli, et al., Phys. Plasmas **6**, 1943 (1998).
22. R. Weynants, G. Van Oost, et al., Nucl. Fusion **32**, 837 (1992).
23. D. Bora, R. S. Ivanov, G. Van Oost, and U. Samm, Nucl. Fusion **31**, 2383 (1991).
24. See the discussion in Ref. 10 and references therein.
25. X. Q. Xu, R. Cohen, G. D. Porter, T. D. Rognlien, D. D. Ryutov, J. R. Myra, D. A. D'Ippolito, R. Moyer, and R. J. Groebner, in *Plasma Physics and Controlled Nuclear Fusion Research 1998* (IAEA, Vienna, 1999), paper IAEA-CN-69/THP2/03.

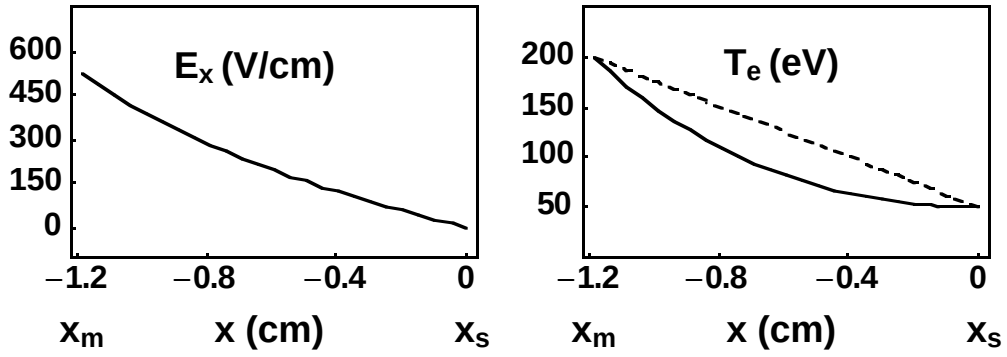

Fig. 1 Solid lines are the equililibrium profiles $E_x(x)$ and $T_e(x)$ satisfying the nonlinear strong-convection constraints, Eqs. (22), in the convective layer ($x_m < x < x_s$). The dashed line is the solution of the heat diffusion equation in the absence of heat sources and sinks, $\nabla_x^2 T_e = 0$.

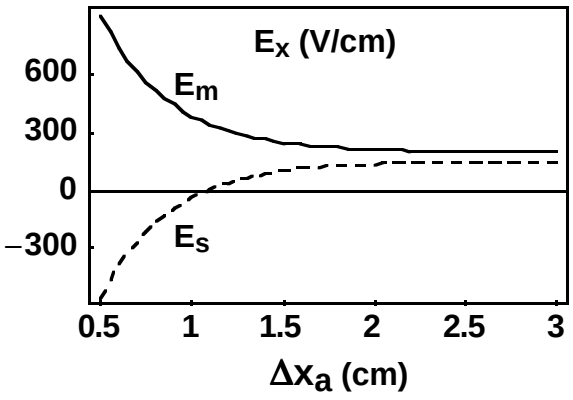

Fig. 2 Plot of electric field at the boundaries of the convective layer, $E_s = E_x(x_s)$ and $E_m = E_x(x_m)$ vs antenna-plasma separation, Δx_a, for parameters typical of the JET 0-phasing ICRF H-mode experiments described in the text. Note that E_s becomes negative and E_m strongly positive for small Δx_a.